Cellulose (2015) 22:2551–2569
DOI 10.1007/s10570-015-0657-4

ORIGINAL PAPER

Biocomposites of polyamide 4.10 and surface modified microfibrillated cellulose (MFC): influence of processing parameters on structure and thermomechanical properties

Agnieszka Leszczyńska · Paweł Kiciliński · Krzysztof Pielichowski

Received: 16 December 2014 / Accepted: 13 May 2015 / Published online: 4 June 2015

Abstract Novel bio-polyamides obtained from renewable resources, *e.g.* PA4.10, are considered nowadays as promising 'green' engineering materials consisting of building blocks derived from castor oil. In this work the composites of heterogeneously acetylated microfibrillated cellulose (MFC) and biopolyamide 4.10 have been prepared by melt blending. Thermoplastic processing of PA4.10/MFC composites was possible in a narrow temperature window due to significant improvement of thermal stability of acetylated MFC as compared to raw MFC. The increase of thermooxidative stability of filler was due to removal of non-cellulosic components from the raw material and introduction of acetic moieties that had additional slight stabilizing effect on MFC. Moreover, the modified MFC showed significant changes in morphology that favoured its dispersibility in viscous polymer melt. Combined treatment of MFC by chemical agents, which caused partial hydrolysis of amorphous regions, and physical disintegration by ultrasonic waves resulted in formation of fibrous material with low degree of entanglement and submicron or nanometric diameters. In the tested range of screw speeds it was found that at screw speed of 100 rpm the shearing forces were sufficient for dispersing MFC agglomerates and the melt pressure secured evacuation of gases introduced to plasticizing system of extruder with MFC-Ac aerogel. The dynamic mechanical properties of obtained (nano)-composites were influenced by both mechanical strengthening of rigid cellulose micro and nanofibers as well as susceptibility of biopolymers towards oxidation and thermomechanical degradation during processing.

Keywords Microfibrillated cellulose · Nanocomposites · Surface modification · Processing · Thermomechanical properties

A. Leszczyńska (✉) · P. Kiciliński · K. Pielichowski
Department of Chemistry and Technology of Polymers, Cracow University of Technology, ul. Warszawska 24, 31-155 Kraków, Poland
e-mail: aleszczynska@chemia.pk.edu.pl
URL: http://www.chemia.pk.edu.pl/wiitch/index.php

Introduction

Due to demands of sustainable development the need for progressive replacement of petroleum based polymers with plastics obtained from renewable raw materials has been widely emphasised. The issue of large volumes of non-biodegradable waste materials is a special concern of *e.g.* packaging industry. In applications where good barrier properties are demanded multilayer films composed of polyolefin and polyamide films are frequently applied. Though this technology offers a good combination of limited permeability of non-polar polyolefins towards water with low permeability of organic vapours through polar polyamide layer, it involves difficulties in recycling of mixed polymer films and has high environmental impact.

In a wide variety of commercially available biopolymers a new group of biopolyamides has recently been introduced on the market. They are obtained in the condensation reaction of diamines and dicarboxylic acids from castor oil (Niaounakis 2015). Importantly, the amount of carbon dioxide emitted during production of PA4.10 is compensated by the amount of CO_2 absorbed during plant growth.

In the group of natural fillers with submicronic and nanometric dimensions the microfibrillated and nanofibrillated cellulose (MFC and NFC, respectively) combine high strengthening potential and good barrier properties (Rodionova et al. 2011). However, due to highly hydrophilic character of the filler interfacial adhesion in polymer/MFC composites is usually not sufficient for proper dispersion of filler and efficient stress transfer during deformation. Numerous methods of surface modification have been recently developed and showed high efficiency in improving dispersibility of MFC and NFC in polymer and strengthening interfacial adhesion leading to better functional properties (Missoum et al. 2011; Miao and Hamad 2013). Despite the promising characteristics of NFC and MFC the application of this group of fillers was basically limited to polymers with low temperature of melting/softening due to insufficient thermal stability of polysaccharide modifiers. As reported in the literature, chemical modification of MFC and NFC influenced the thermal stability of material. However, only few works reported an increase of thermal stability of nanocellulose by *e.g.* surface acetylation (Nogi et al. 2006) or silanization (Qua et al. 2011).

In this work MFC was submitted to heterogeneous acetylation by acetic anhydride, then characterised and used for preparation of a new type of micro/nanocomposites based on a biopolyamide-PA4.10. The effects of processing conditions on the dispersion degree of modified MFC as well as on the thermal and dynamic mechanical properties of PA4.10/MFC composites were investigated.

Experimental

Materials

Microfibrillated cellulose under the commercial name Arbocel MF 40-7 was kindly supplied by J. Rettenmeier and Shöne GmbH + CO KG in the form of water dispersion with 7 wt% content of dry MFC. Average particles size distribution of the cellulose fibrils in dispersion was approx. 70–200 nm (Rettenmaier 2012). Reagent grade acetic anhydride and pure solvents used in solvent exchange process were obtained from Sigma-Aldrich and used as delivered. Polyamide 4.10 applied in this work was an engineering polymer produced by DSM under commercial name EcoPaXX Q-170MS. EcoPaXX® is 70 % made from renewable materials (castor oil) and is 100 % carbon neutral. The properties of applied PA4.10 were: melt flow index (MFI) 24 g/10 min, viscosity number 170 cm^3/g and melting temperature (10°/min) 250 °C (DSM 2014).

Preparation of modified MFC

The water dispersion of raw MFC was solvent exchanged to acetone and then to toluene by successive centrifuging and dispersing of obtained sediment by ultrasonic homogenizer in fresh portion of solvent. For each solvent the procedure of centrifuging and dispersing was carried out for three times. In each operation step the pulsatory sonication was applied for avoiding the overheating and local evaporation of volatile solvent. The acetylation of 2 g of microfibrillated cellulose by acetic anhydride was carried out in 100 ml of toluene (analytical grade) at 70 °C under continuous stirring and continuous flow of argon. After the initial mixing of MFC dispersed in toluene and stabilization of temperature (approx. 20 min), the proper amount of acetic anhydride was drop-wise added to the reaction system. The reaction time was 120 min and the molar ratio of total cellulose hydroxyl groups to acetic anhydride (OH:AA) was 1:10 according to previously reported work on optimization of cellulose modification procedure (Leszczyńska et al. 2013). Immediately after the modification, the cellulose was solvent exchanged back to water. In subsequent washing steps unreacted anhydride and side products, *e.g.* acetic acid, were removed.

A portion of MFC was subjected to all steps of solvent exchange procedure (from water to acetone and toluene, and then back from toluene through acetone to water), as well as sonification and centrifuging, but not submitted to chemical reaction with acetic anhydride. This material was denoted as MFC SolEx. All samples of MFC were freeze-dried and then blended with PA4.10 in the Mini CTV, a conical type

laboratory twin screw extruder produced by Thermo Electron Corporation. The barrel of the screw is equipped with the bypass that allows the polymer melt to be recirculated from the end of the metering section back to the feeding section. Through this configuration the dwell time in the extruder can be extended and flexibly controlled. The cellulose-based filler was introduced into the already melted polymer to limit its thermooxidative degradation. The time of mixing of MFC with PA4.10 was 3 min for all prepared samples. Total dwell time of PA4.10 in extruder, including the time of polymer plasticization, was 7 min.

Description of PA4.10/MFC composites produced under different rotational screw speeds is given in Table 1.

Techniques

Wide angle X-ray diffraction (WAXD) analysis was performed using a Philips X Pert diffractometer ($\lambda_{Cu} = 1.54$ Å). Thermogravimetric analysis (TGA) was performed by applying a Netzsch TG 209 thermal analyser, operating in dynamic mode at a heating rate of 10 K/min. The conditions were: sample weight $\sim$5 mg, atmosphere—air, open α-Al_2O_3 pan. Fourier transform infrared spectra have been recorded on freeze dried cellulose using a BIORAD FTS 165 spectrometer equipped with ATR attachment [FTIR-attenuated total reflection (ATR)], operating in the spectral range of wavenumber of 4000–400 cm^{-1}. Scanning electron microscopy (SEM) pictures were taken with the Jeol JSM-6010LA apparatus. High resolution of this microscope enables observation of nanostructures as small as 3.0 nm at 30 kV. Prior to SEM observations, the polymer samples were fractured immediately after immersion in liquid nitrogen and then brittle fracture surfaces were sputter-coated with gold using an SPI sputter coater. The dynamic laser scattering (DLS) measurements were carried out on Malvern Zeta Sizer Nano ZS. The detection was made at a scattering angle of 173° and the intensity size distributions were obtained with the apparatus software using the CONTIN algorithm. The suspension concentration was 0.5 mg/ml for both samples. Samples were sonicated for 2 min in order to prepare a proper dispersion of particles in water and then stabilized for 60 min. The scattering cell was thermostated at 25 °C. The investigations of melting and fusion of PA4.10/MFC composites were performed using a DSC Netzsch 200 under the following conditions: temperature range −50 to 200 °C, heating/cooling rate of 10 °C/min, sample mass *ca.* 5 mg. Dynamic mechanical analysis of extruded composite profiles with cross-section dimensions of 3.0 × 2.5 mm was performed using a Netzsch 242 C DMA analyzer operating in a three-point bending mode in the temperature range of −160 to 150 °C. The heating rate was 2°/min., free bending length was 40 mm and the aim amplitude was set at 100 μm.

Results and discussion

Characterization of heterogeneously acetylated MFC

Structural analysis of the cellulosic filler by FTIR-ATR spectroscopy

The FTIR-ATR spectra of acetylated MFC show new peaks not observed in the spectrum of raw MFC. Two peaks at 1733 cm^{-1}, that are related to the stretching vibrations of carbonyl group (ν C=O), and a peak at 1249 cm^{-1} due to stretching vibrations of C–O bond

Table 1 Description of PA4.10/MFC composites produced under different rotational screw speeds

MFC-Ac content (wt%)	Rotational screw speed (rpm)		
	50	100	150
0	PA_50	PA_100	PA_150
1	PA/MFC-Ac 1 %_50	PA/MFC-Ac 1 %_100	PA/MFC-Ac 1 %_150
3	PA/MFC-Ac 3 %_50	PA/MFC-Ac 3 %_100	PA/MFC-Ac 3 %_150
5	PA/MFC-Ac 5 %_50	PA/MFC-Ac 5 %_100	PA/MFC-Ac 5 %_150

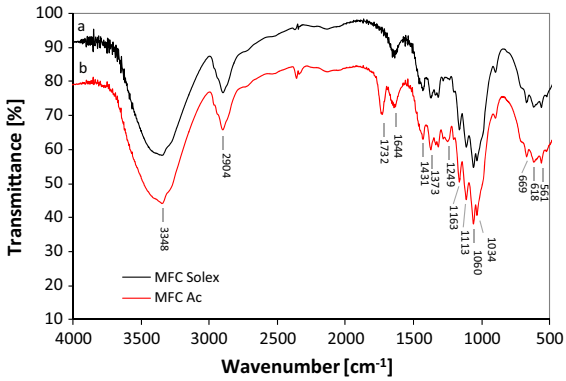

Fig. 1 FTIR spectra of *a* unmodified MFC after complete solvent exchange procedure and *b* heterogeneously acetylated MFC (MFC-Ac)

in ester group, clearly demonstrate partial esterification of MFC (Fig. 1). The intensity of peaks is not very strong and indicates low substitution degree of cellulose hydroxyl groups, probably limited to the most reactive hydroxyl groups at C2 and C6 in cellulose mer (Eyley and Thielemans 2014). Strong peaks at 1063 and 1160 cm^{-1} are related to C–O and C–O–C stretching vibration in cellulose, respectively (Fengel 1993; Gierlinger et al. 2006). Another broad peak at 1644 cm^{-1} was attributed to the bending vibrations of adsorbed water.

The band appearing between 3700 and 3100 cm^{-1}, which is derived from OH-stretching vibrations, comprises several distinct bands related to cellulose hydroxyl groups forming inter- and intra-molecular hydrogen bonds, free cellulose hydroxyl groups and absorbed water (Hinterstoisser and Salmén 2000; Ali et al. 2001).

Analysis by SEM and DLS

The morphology of raw MFC and MFC-Ac was analysed by SEM (Figs. 2, 3). Raw MFC is comprised of anizometric cellulose particles with a wide range of diameters from 1 to 30 µm and low aspect ratio. The chemical modification resulted in major change in material morphology. Microfibers with submicronic diameter and complex morphology exposing individual cellulose crystals became dominant fraction of material. Particles evidenced features of microcrystalline cellulose but nanocrystals were kept in the fibrillar arrangement. Changes in MFC morphology could arise as simultaneous action of chemical process of hydrolysis in acidic environment and physical disintegration, especially of larger particles, during repeated sonication.

Microscopic observations provided only qualitative assessment of the materials' morphology. SEM microscopy did not allow to determine the reliable values of the fibrils length and diameters distribution by picture analysis due to the entanglement of fibrils. The morphological features of MFC Solex and MFC-Ac samples were also studied by the dynamic light scattering (DLS) method. The results of DLS analysis are presented in Fig. 4.

The dispersions of both unmodified (MFC Solex) and acetylated MFC (MFC-Ac) in water exhibited bimodal size distribution with high contribution of particles with the hydrodynamic diameters around few micrometers. The size distribution profile of acetylated MFC indicated a slight shift towards lower sizes for both fractions. Despite of high demand, the standard methods or validated techniques for the size

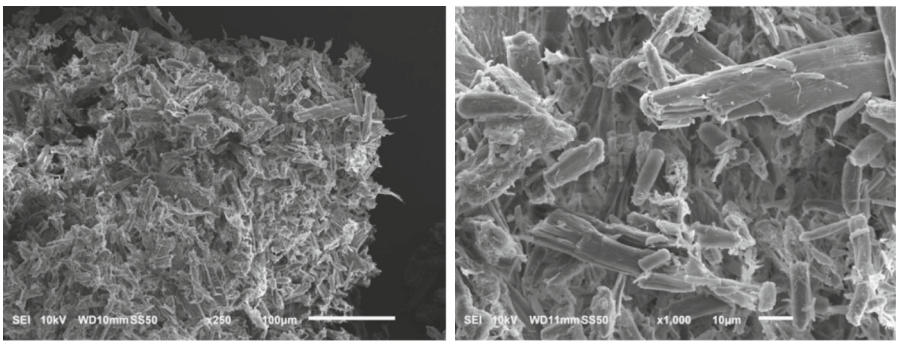

(a) 250x **(b)** 1000x

Fig. 2 SEM microphotographs of raw MFC at magnification **a** ×250 and **b** ×1000

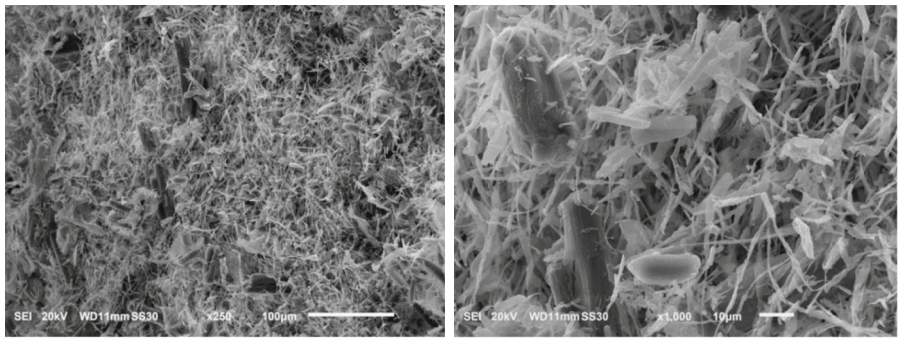

(a) 250x **(b)** 1000x

Fig. 3 SEM microphotographs of surface modified microfibrillated cellulose (MFC-Ac) at magnification **a** ×250 and **b** 1000×

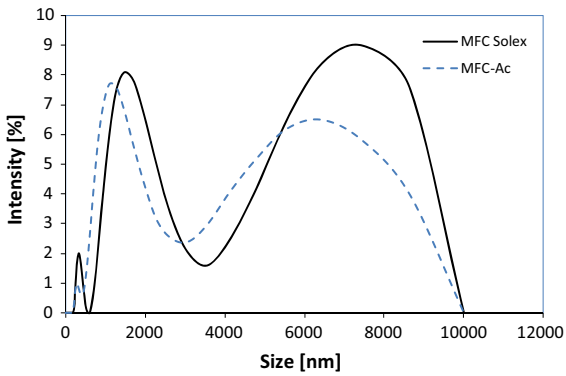

Fig. 4 Intensity distributions obtained by dynamic light scattering for MFC-Solex and MFC-Ac water suspensions

evaluation of polydisperse nanomaterials with a high aspect ratio, including cellulose nanocrystals and nanofibrils, are still under development (Gamelas et al. 2015; Fraschini et al. 2014). In the very recent work by Gamelas et al. the DLS hydrodynamic diameter, as an equivalent spherical diameter, was used to estimate the nanofibrils length assuming a cylinder with the same volume and with the diameter (width) assessed by AFM (Gamelas et al. 2015). In the work by Fraschini et al. with the anizometric cellulose microfibrils or whiskers, the hydrodynamic radius determined by DLS was considered only as an indicative measure of the 'apparent' size of the dynamic hydrated/solvated particle (Fraschini et al. 2014). It was also pointed that in the case of rod-like particles, such as cellulose nanocrystals, a slight change in the length will directly affect the measured DLS size while changes in the cross-section will hardly affect the diffusion velocity. In other words, the DLS method would rather provide information on the length distribution of the nanocellulose fibers and is significantly less sensitive to the diameter variations that were observed on SEM microphotographs. Besides, several other significant limitations of the DLS method must be taken in consideration when interpreting the results. Most important are possible agglomeration of nanosized particles and relatively high content of micrometric agglomerates that may produce multiple scattering. The MFC microparticles might origin from a raw material as well as arise due to agglomeration of nanofibrils during drying or due to hydrogen bonding in the water suspension. Interestingly, Builes and co-workers demonstrated by that by adding an effective surfactant to the water suspension of microfibrillated cellulose the particles diameters, determined by DLS method, were significantly reduced (Builes et al. 2013). The authors explained this phenomenon by surfactant-MFC interactions that prevented formation of larger agglomerates in water environment.

SEM analysis of the MFC indicated significant decrease of particles diameters in the course of chemical treatment while the fiber length was basically preserved, as determined by the DLS method. However, agglomerates displayed by SEM and DLS analysis in the filler were broken into smaller individuals under high shears during melt blending of PA4.10/MFC-Ac composites, as it is discussed in the following part of the study.

WAXD analysis of modified MFC

The influence of chemical modification of MFC by heterogeneous acetylation on crystal structure of

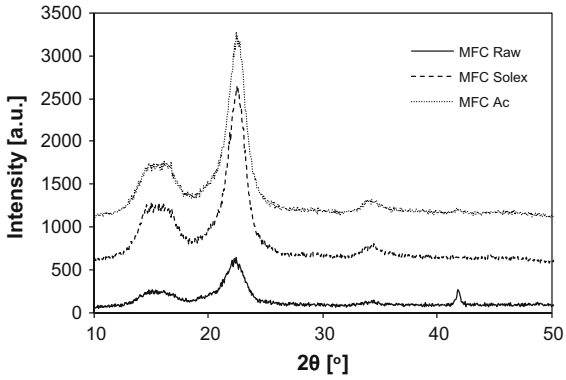

Fig. 5 WAXD diffraction patterns of MFC, MFC SolEx that underwent complete solvent exchange process and MFC-Ac that was surface modified by acetic anhydride

Table 2 Crystallinity degree (X_{CR}) of MFC samples

Sample	Crystallinity degree X_{CR} (%)
MFC Raw	80.77
MFC SolEx	86.61
MFC-Ac	81.07

fibrils was estimated by WAXD method. Diffraction patterns of raw MFC, MFC SolEx, and MFC-Ac are collected in Fig. 5.

Crystallinity degree of cellulosic materials was determined according to Segal method (Segal et al. 1959) based on the following equation:

$$X_{CR} = \frac{I_{002} - I_{AM}}{I_{002}} \times 100\,\% \quad (1)$$

where X_{CR}—crystallinity index (%); I_{002}—intensity of diffraction peak in the range of 22°–24° corresponding to 002 crystal plane, I_{AM}—intensity of the minimum at $2\theta = 18°$, which is approximated value of amorphous halo.

The highest crystallinity degree was found in MFC after solvent exchange process (Table 2). This finding indicates extraction of non-crystalline components from the raw MFC material, such as other carbohydrates that naturally occur in the wood pulp, whereby less contaminated crystalline cellulose fibrils remain after repetitive washing. Acetic anhydride action caused only a slight decrease in MFC crystallinity degree as compared to MFC-SolEx. WAXD and FTIR data indicate that the esterification reaction occurred in amorphous regions of microfibrils and on the surface of cellulose crystals, while the core of crystallites remained unchanged. Literature survey on chemical modifications of cellulose nanocrystals shows that relatively small loss of crystallinity can be achieved at moderate concentration of modifier and limited time of reaction (Eyley and Thielemans 2014). Significant damage to the crystal structure for esterified cellulose nanocrystals can be expected at high surface substitution degree (DS_{surf}) of 1.5 (Braun and Dorgan 2009). The preservation of MFC crystalline structure during modification is crucial for maintaining its reinforcing potential, as well as barrier properties.

The values of X_{CR} obtained for MFC materials used in the course of this work are similar to that reported in literature, for example for nanocellulose extracted from sisal fibers (Morán et al. 2008). The X-ray diffraction analysis methods, including Segal method, are convenient and widely used for estimation of crystallinity index (CI) of cellulose micro- and nanoparticles (Terinte et al. 2011). However, the simplified character of this method (Park et al. 2010), the influence of disorder in cellulose fibrils (Lindner et al. 2015) and different crystallite dimensions (Leppänen et al. 2009; French and Cintrón 2013) have recently been pointed as sources of significant errors. Nevertheless, Segal's method is applicable for empirical measurements that allow direct comparison of cellulose-based materials and determination of trends.

Thermooxidative degradation of modified MFC

The process of thermooxidative degradation of MFC fillers was evaluated by thermogravimetric method. At temperatures below 120 °C the mass loss was due to moisture vaporisation. The initial temperature of thermooxidative degradation for unmodified microfibrillated cellulose was *ca.* 277 °C, which is within the processing temperature range of polyamides. Thus, successive preparation of composite materials based on PA with raw MFC by melt blending is impossible. Serious degradation of cellulose-based fillers should be expected especially when polyamide 4.10 is applied as a composite matrix due to its relatively high melting temperature. Solvent exchange procedure itself induced significant changes in the thermooxidative stability of MFC, especially in the initial stage of the decomposition process, which is crucial for processability of filler and preservation its beneficial mechanical and barrier properties during melt blending. For MFC SolEx one can observe an increase of thermooxidative stability

displayed as an increase in the onset temperature of degradation by over 35 °C and temperature at 10 % mass loss by about 11 °C (Table 3). Surface modification of MFC by acetylation caused further slight increase of the initial degradation temperature. The degradation process of all three MFC occurred in two stages. In the main degradation step (I) the temperatures at maximum rate of mass loss were not shifted by the physical processing and only slightly increased by the chemical modification. However, the overall course of the decomposition in this stage was visibly altered. The degradation of solvent exchanged and acetylated MFC was rapidly accelerated in a narrow temperature range as displayed in the DTG curves (Fig. 6). The second stage of degradation proceeded similarly in both modified samples but was shifted to higher temperatures.

The observed substantial changes in the thermooxidative degradation of MFC after solvent exchange procedure is most probably due to extraction of carbohydrate components (with higher susceptibility to thermooxidative degradation) from the raw product by repeating washing. The raw cellulose pulp used for MFC production is a complex material with cellulose as a main component, but containing also lignin, hemicelluloses and in some cases pectins (Dufresne 2012). Pure crystalline cellulose is expected to present higher thermal stability due to regular crystalline structure and lack of less stable functional groups such as carboxyl groups prone to decarboxylation.

Influence of processing parameters and MFC content on the composite structure and morphology

Morphological studies by microscopic techniques

The attempt to obtain a PA composite material with unmodified raw MFC failed due to severe degradation

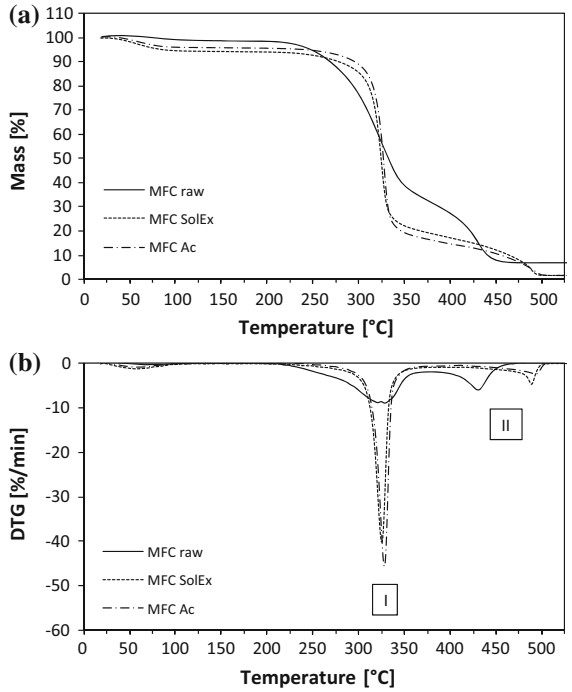

Fig. 6 **a** TG and **b** DTG profiles of raw MFC, MFC after solvent exchange (MFC SolEx) and surface modified MFC (MFC Ac)

of components but compounding of PA4.10 with MFC after complete solvent exchange procedure and acetylated MFC allowed production of composite material suitable for further tests. Moreover, surface modification clearly enhanced the dispersibility of MFC in PA4.10 matrix and improved the appearance quality of the extruded rods, as evidenced by optical microscope photographs taken in a reflected light mode (Fig. 7).

The microstructure of PA4.10 surface showed typical brittle fracture of polymer material without distinctive structures (Fig. 8). SEM pictures of cryofractured profiles of PA4.10/MFC-Ac-3 % composite produced at different screw speeds are presented in

Table 3 Results of thermogravimetric analysis of MFC fillers

Sample	Degradation step	T_{max} (°C)	Mass loss (%)	T_{onset} (°C)	$T_{10\%}$ (°C)	$T_{50\%}$ (°C)	Char at 600 °C (%)
MFC Raw	I	324.2	59.71	277.6	267.5	332.2	7.13
	II	430.3	33.22				
MFC SolEx	I	324.8	73.68	313.1	279.1	324.2	1.73
	II	488.1	24.44				
MFC Ac	I	327.6	77.10	316.5	294.1	326.5	1.62
	II	492.5	21.03				

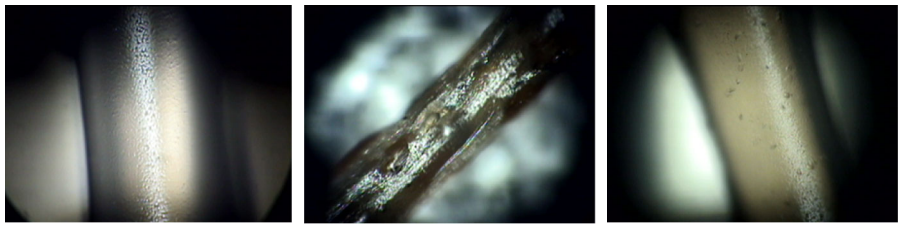

(a) PA_100 **(b)** PA/MFC Raw 3%_100 **(c)** PA/MFC-Ac 3%_100

Fig. 7 Macro photographs of **a** neat PA4.10, **b** PA/MFC-Raw 3 % and **c** PA/MFC-Ac 3 % extruded rods

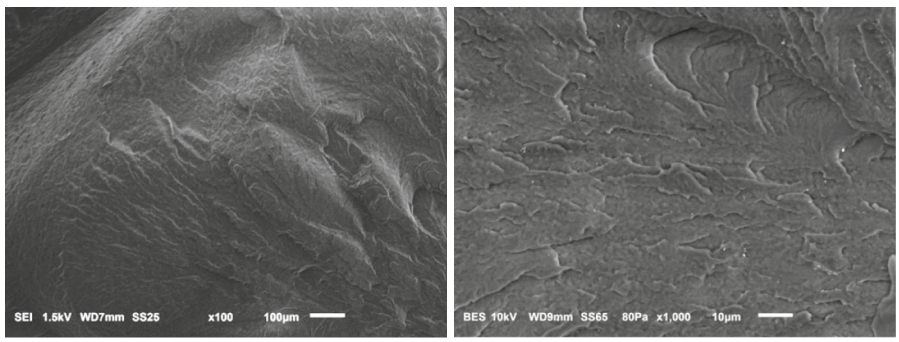

PA410_100

Fig. 8 SEM pictures of neat PA 4.10 cryofractured profile

Fig. 9. Both cellulose filler and polyamide matrix are organic polymers and comprise elements having similar atomic mass. Thus, under SEM observation MFC is not very well visible phase. However, differences in carbon and oxygen content between components as well as presence of nitrogen atom in polymer matrix produce sufficient material contrast and allow analysis of composites structure and morphology. Microfibrillated cellulose after modification was mainly composed of rigid linear particles which after processing could be visible in PA matrix as straight whisker-like fibers with regular boundaries. This was a specific morphological feature distinguishing MFC particles from the less regular cracks present in the polyamide matrix.

At screw speed of 50 rpm the microfibrillated cellulose was not sufficiently dispersed in the PA matrix and numerous agglomerates with sizes up to 80 µm were observed (Fig. 9). Also small voids/bubbles were formed as gases could be entrained in the cellulose powder and were not sufficiently evacuated from the extruder under moderate melt pressure generated at low rotational screw speed. Moreover, moisture and volatile products of degradation could be evolved from both polymeric components during melt blending. At higher screw speed one can observe much better dispersion and distribution of micro/nanocellulose particles. Some of them were depicted with arrows in the Fig. 9. Agglomerates and other defects are rather rare in PA/MFC-Ac-3 %_100 material but gas bubbles are more likely to occur in material processed at 150 rpm. Particles of acetylated MFC observed on the fracture surfaces are partially covered with PA which indicates rather good interfacial adhesion.

At higher content of MFC-Ac (5 wt%) the defects, especially gas bubbles, were more frequently observed (Fig. 10). The apparent density of microfibrillated cellulose aerogel is very low and it comprises mainly air which can easily be captured by polymer melt. Processing of such materials by melt blending requires effective degassing system. Larger number of cavities and bubbles might be also indicative of higher extent of thermomechanical degradation corresponding to increased content of thermally sensitive material. The least defects were observed in composite containing 3 wt% and prepared at screws speed of 100 rpm. However, the dispersion and equal distribution of individual MFC particles increased with the screw speed. The final mechanical and barrier performance of biopolyamide/MFC composites is expected to

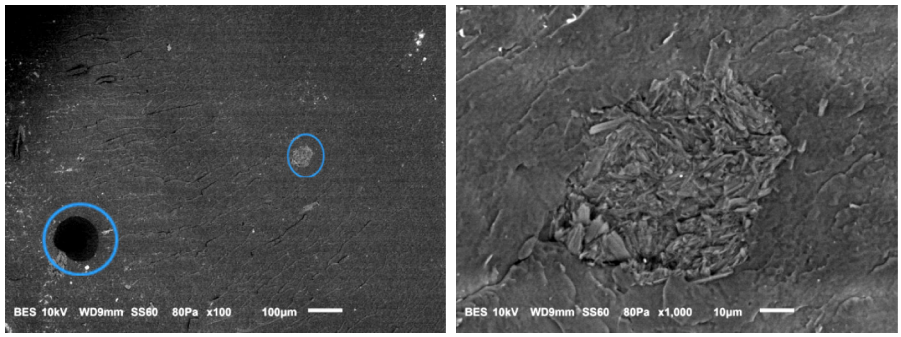

(a) PA/MFC-Ac-**3%_50**

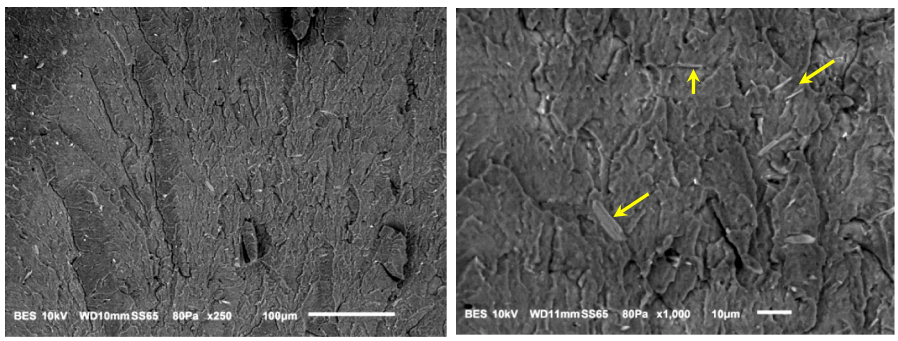

(b) PA/MFC-Ac-**3%_100**

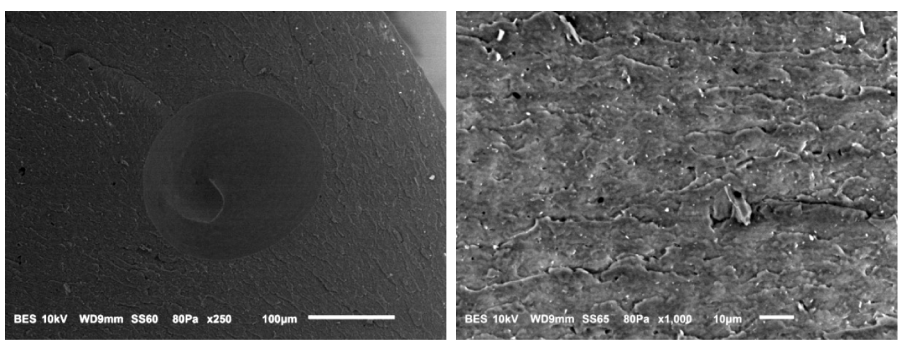

(c) PA/MFC-Ac-**3%_150**

Fig. 9 SEM microphotographs of PA/MFC-Ac 3 % micro/nanocomposites obtained at different screw speeds: **a** 50 rpm, **b** 100 rpm, **c** 150 rpm

depend on homogenization degree of submicronic filler and the presence of morphological defects of different origin.

SEM microphotographs of a series of PA/MFC-Ac 1 % composites (not shown here) reveal the presence of voids and agglomerates, however, there are less individual MFC particles due to small amount of additive.

Generally, at screw speed of 50 rpm the mixing intensity and backpressure were not sufficient for producing bio-PA/MFC composites with good quality. The higher screw speed was applied the better dispersion degree of MFC in PA4.10 matrix was achieved. The highest number of cavities and gas bubbles was observed at screw speed of 50 rpm. The smaller number of defects was revealed in composites produced at 100 rpm but a further increase of the screws speed up to 150 rpm again resulted in generating of considerable number of bubbles. Defects observed at the highest screws speed resulted probably from local overheating of the melt and thermomechanical degradation of polymers during processing.

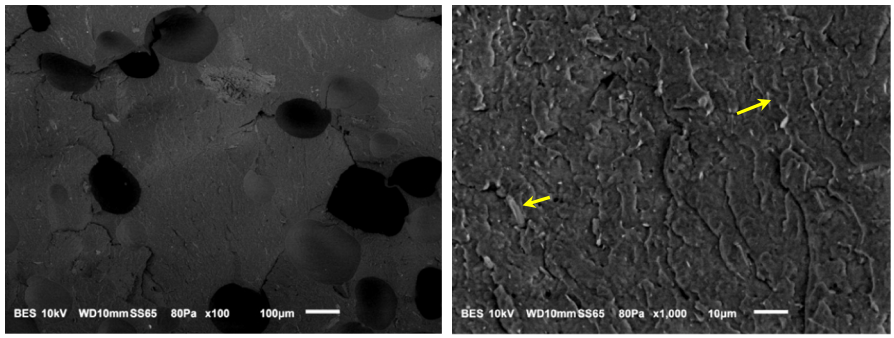

(a) PA/MFC-Ac-**5%_50**

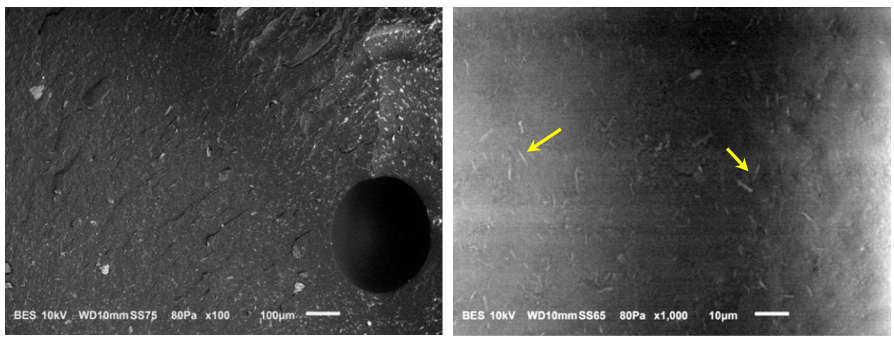

(b) PA/MFC-Ac-**5%_100**

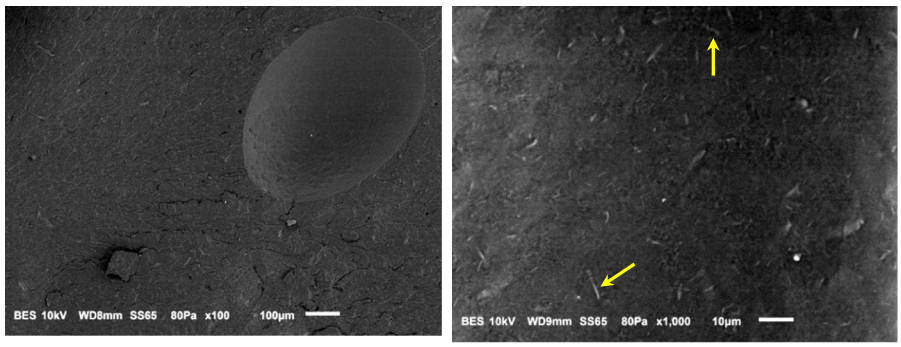

(c) PA/MFC-Ac-**5%_150**

Fig. 10 SEM microphotographs of PA/MFC-Ac 5 % micro/nanocomposites obtained at different screw speeds: **a** 50 rpm, **b** 100 rpm, **c** 150 rpm

Taking into account morphological results one can indicate that processing of temperature sensitive cellulosic filler with bio-PA engineering polymers is a challenging issue, however, it was proved to be possible if proper modification procedure is applied. During the processing of PA4.10/MFC composites the highest possible intensity of mixing that promotes the dispersion of MFC in PA matrix, had to be compromised with the control of excessive heat released due to friction. Further adjustment and control of temperature providing efficient plasticization, homogenization and preventing of material degradation at high throughput can be achieved on the semi-industrial extrusion lines usually equipped with multiple heating and cooling zones and vacuum degassing systems. With growing melt viscosity of the polymer the risk of overheating during processing is higher as a result of more intensive shearing. Thus, melt blending of thermally sensitive MFC or NFC with low viscosity engineering resins would be easier to control. Lower viscosity of polymers and lower molecular weight was reported to favour the dispersion of nanoadditives and

this effect was explained by faster melt infiltration by primary agglomerates (Kasaliwal et al. 2011a, b). Therefore different viscosity grades of PA4.10 would be required for industrial applications, such as automotive industry (injection moulded parts, for example engine covers) and packaging sector (extrudable and film forming grades for plastic films with improved barrier properties and balanced CO_2 index).

FTIR analysis of composites

The FTIR spectra of PA4.10/MFC-Ac nanocomposites prepared under different processing conditions with varying MFC content are presented in Figs. 11 and 12. Due to low content of the filler the infrared spectra of composite materials do not differ much from that taken for the pristine polyamide 4.10. However, several additional bands and changes in intensity of existing bands have been observed in composites spectra. Hence, with the increasing content of MFC-Ac a gradual increase of absorption intensity in carbonyl region at 1742 cm^{-1} was observed. Therefore, this band was correlated with the carbonyl stretching vibrations in cellulose acetate at 1734 cm^{-1} (see Fig. 1). Other absorption bands associated with the modified cellulose in biopolyamide matrix were observed at 1034, 1060 and 1113 cm^{-1}, especially in spectra of nanocomposites containing 5 wt% of filler. The bands at 1007 and 1046 cm^{-1} in the PA4.10 (Figs. 11, 12) are in the spectral range of C–C skeletal stretching vibrations of aliphatic polyamides (Luo et al. 2011). In polyamide 6.10, a homolog to PA4.10, typical absorption bands occur at 1480, 1245 and 940 cm^{-1} (Ogava and Fujiwara 1985). The strong absorption band at 3299 cm^{-1}, due to stretching vibrations of N–H bound in polyamide, overlaps the stretching vibrations of hydroxyl groups in cellulose. Therefore no significant change can be detected in that region. However, we observed some weak bands which do not overlap strictly with the absorption maxima of pure components. In carbonyl region one can find additional peaks at 1711 and 1729 cm^{-1}. There is probably a shift of absorption frequency for C=O group either in acetylated cellulose or in polyamide due to formation of specific interactions between the components. Polyamide macrochains can form hydrogen bonds with cellulose in the interfacial layer. However, the fraction of filler macromolecules located on the interface is probably not large with respect to total mass of the filler so the polymer matrix-polymer additive interactions are rather weak. Strong changes in FTIR spectra were observed in polyamide-based systems containing low molecular weight additives capable to overcome high cohesion energy E_c of polyamides by destroying its hydrogen bonding and forming interactions with amide groups on a molecular level (Roberts and Jenekhe 1991; Afshari et al. 2008).

On the spectra of PA4.10/MFC-Ac composites some small additional bands contributed to C–C skeletal absorption region at 1020 and 1049 cm^{-1} can be observed. Changes in the spectra could also reflect formation of additional carbonyl compounds as a result of thermomechanical degradation or oxidation of components during melt blending, as both biopolymers are susceptible to oxidation. Generally, raw materials used in this work are biopolymers with relatively high degree of crystallinity and a major part of biopolyamide as well as cellulose macromolecules form crystals with intra- and inter-molecular H-bonds.

Studies of polyamide phase transitions in PA4.10/MFC-Ac composites by DSC

Bio-PA/MFC composites containing different amounts of MFC-Ac and manufactured in different processing conditions displayed characteristic changes in the melting and crystallization behaviour as evidenced by DSC analysis (Table 4).

A slight decrease of melting temperature was observed with an increase of MFC content (Fig. 13). This effect indicates the formation of smaller and less perfect crystallites of PA4.10 in the presence of MFC-Ac. PA4.10/MFC-Ac materials are two phase systems comprising two crystalline polymers and thermal behaviour of polyamide matrix is influenced by the presence of another polymer—a filler. In polymer blends similar effects were interpreted as a result of H-bond formation between polymeric compounds. Higher order interactions increase miscibility of blend components but interfere with the formation of perfect crystals (Zhu et al. 2004; He et al. 2001a, b). A decrease of melting temperature T_m in semicrystalline polymers brings important information about miscibility and its associated with polymer–polymer interaction parameter χ_{12} (He et al. 2004). It was explained by thermodynamic depression related to a decrease in the chemical potential due to the presence of the

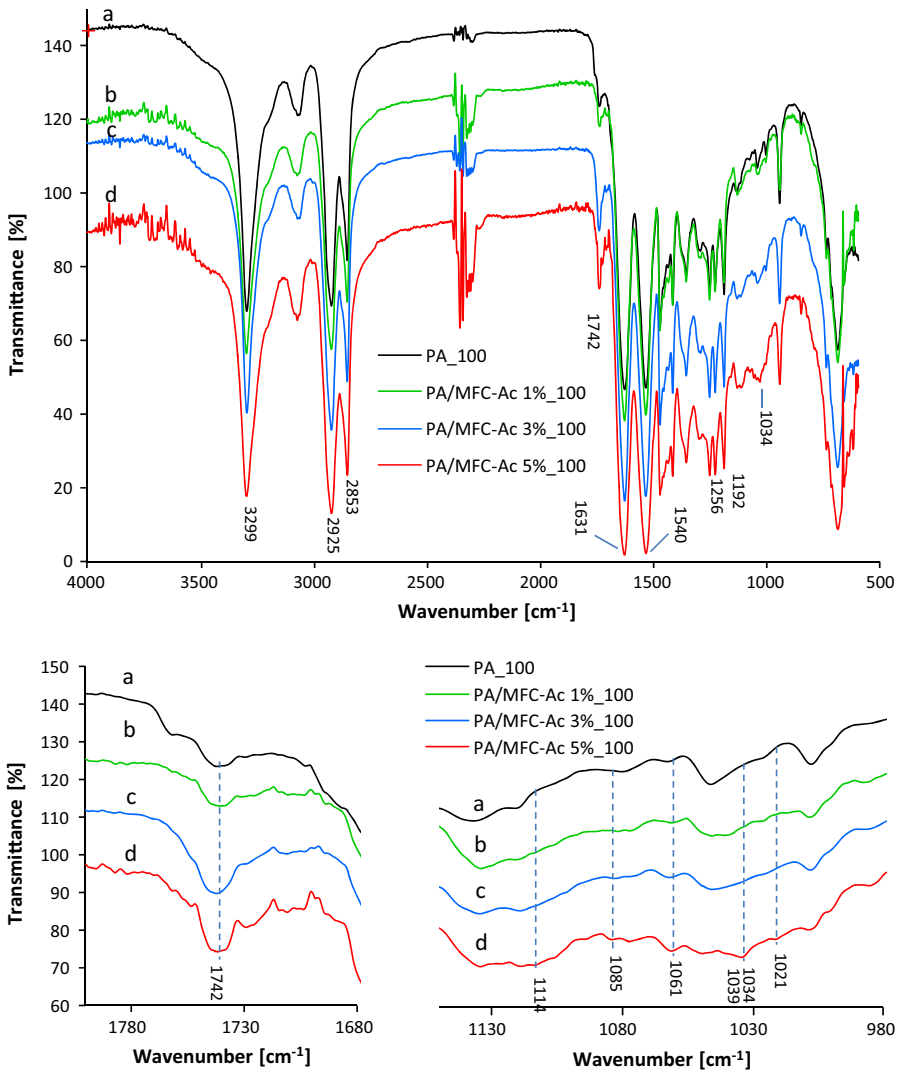

Fig. 11 FTIR spectra of pure PA4.10 and PA4.10/MFC-Ac nanocomposites with varying filler content prepared at rotational screw speed of 100 rpm: *a* pure PA4.10, *b* PA/MFC-Ac 1 %_100, *c* PA/MFC-Ac 3 %_100, *d* PA/MFC-Ac 5 %_100

polymeric solvent. When two polymers are miscible in the melt, the chemical potential of the crystallizable polymer is decreased due to the addition of the second component. Melting point depression was typically observed in hydrogen-bonded blends if the blend contained a semicrystalline component (Li et al. 2001; He et al. 2001a, b). The degree of mutual interactions of both components in PA4.10/MFC-Ac depends on the interfacial surface arising from the dispersion level. Melting of PA4.10 in composite systems subjected to higher shearing at rotational screw speed of 150 rpm occurred in slightly wider temperature range. This effect may also origin from an increase of molecular weight distribution due to processing operations.

Crystallization temperature of PA4.10 (Fig. 14) was slightly shifted towards higher temperatures by addition of MFC-Ac indicating heterogeneous nucleation of crystallization induced by cellulose filler. The least overcooling to undergo crystallization was necessary for composites with 5 wt% of MFC-AC. The onset temperature of crystallization showed minor changes only for selected composites. The crystallinity degree (Table 4) of polyamide in composites was calculated according to the formula:

$$X_{cDSC}(\%) = \frac{\Delta H_m}{\left[(1-\phi)\cdot \Delta H_m^0\right]} \times 100\,\% \qquad (2)$$

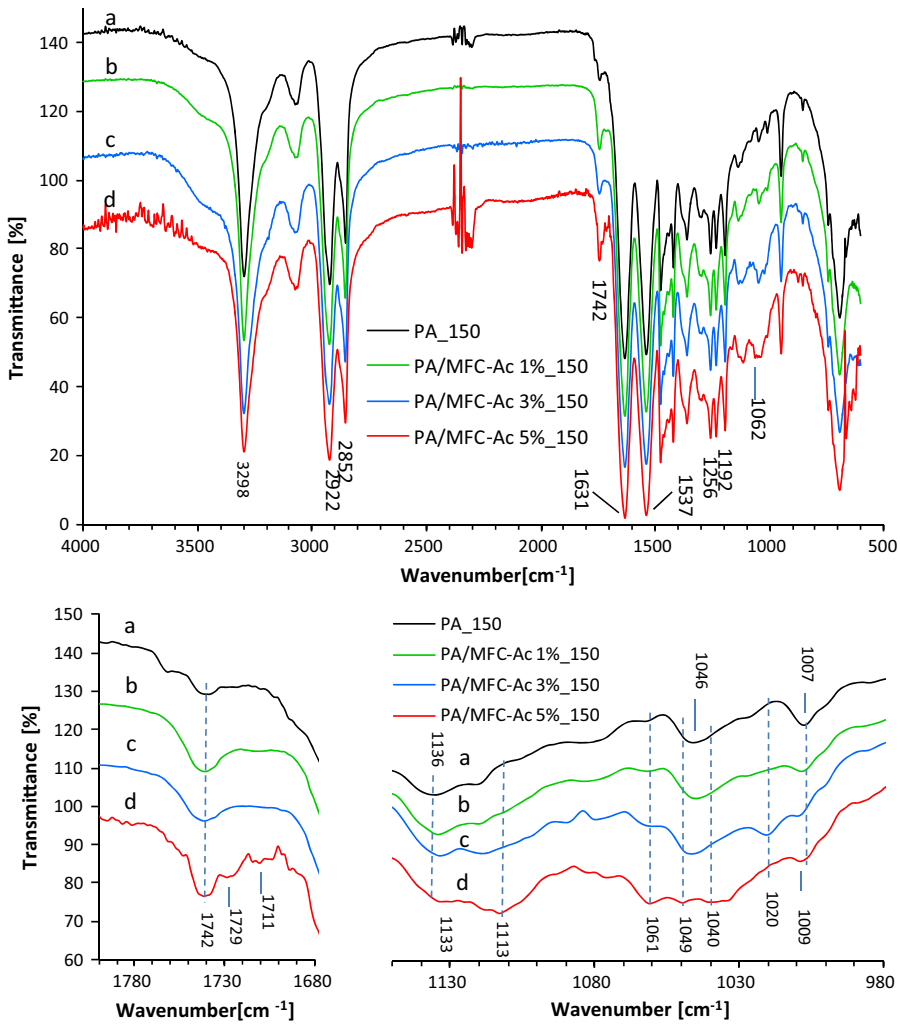

Fig. 12 FTIR spectra of pure PA4.10 and PA4.10/MFC-Ac nanocomposites with varying filler content prepared at rotational screw speed of 150 rpm: *a* pure PA4.10, *b* PA/MFC-Ac 1 %_150, *c* PA/MFC-Ac 3 %_150, *d* PA/MFC-Ac 5 %_150

Table 4 Results of DSC analysis of PA/MFC-Ac composites

Sample	ΔH_m (J/g)	T_m (°C)	T_C (°C)	T_{Conset} (°C)	X_{CDSC} (%)
PA_50	−69.74	246.67	222.76	238.44	35.4
PA/MFC-Ac 1 %_50	−68.81	246.67	222.92	239.07	35.3
PA/MFC-Ac 3 %_50	−69.00	245.83	223.13	238.17	36.1
PA/MFC-Ac 5 %_50	−69.07	246.00	223.44	238.45	36.9
PA_100	−71.67	247.17	222.53	237.45	36.4
PA/MFC-Ac 1 %_100	−68.61	246.54	222.72	238.73	35.2
PA/MFC-Ac 3 %_100	−68.67	246.13	222.60	237.91	35.9
PA/MFC-Ac 5 %_100	−69.75	245.31	223.46	237.64	37.3
PA_150	−72.83	246.67	222.72	237.58	37.0
PA/MFC-Ac 1 %_150	−70.65	246.39	222.90	237.29	36.2
PA/MFC-Ac 3 %_150	−67.75	246.42	222.85	237.48	35.5
PA/MFC-Ac 5 %_150	−69.01	245.71	223.36	237.78	36.9

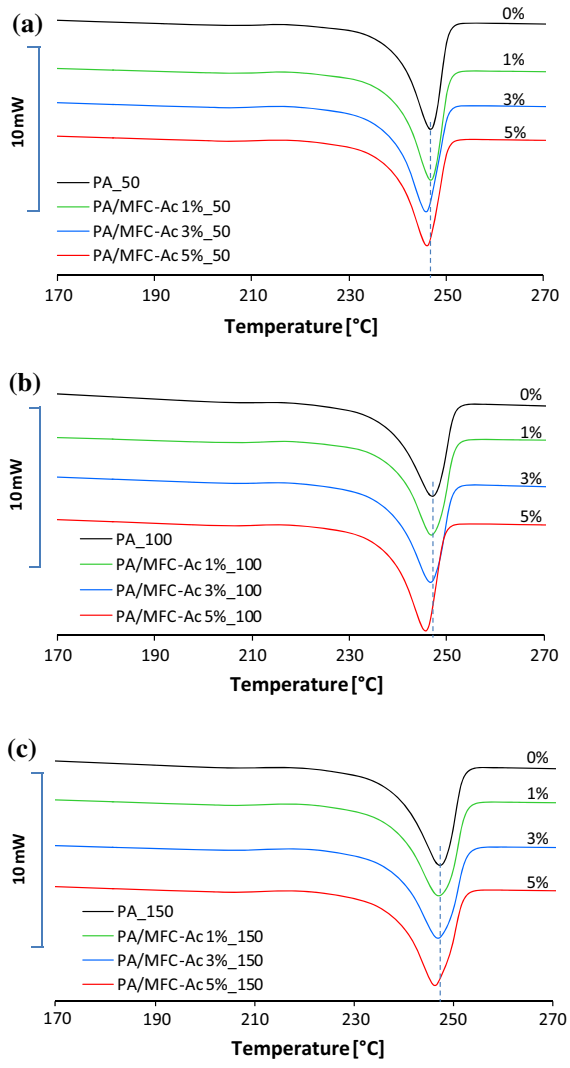

Fig. 13 DSC endotherms of second heating scan for biopolyamide composites with varying MFC-Ac content and manufactured at different screws speeds: **a** 50 rpm, **b** 100 rpm, **c** 150 rpm

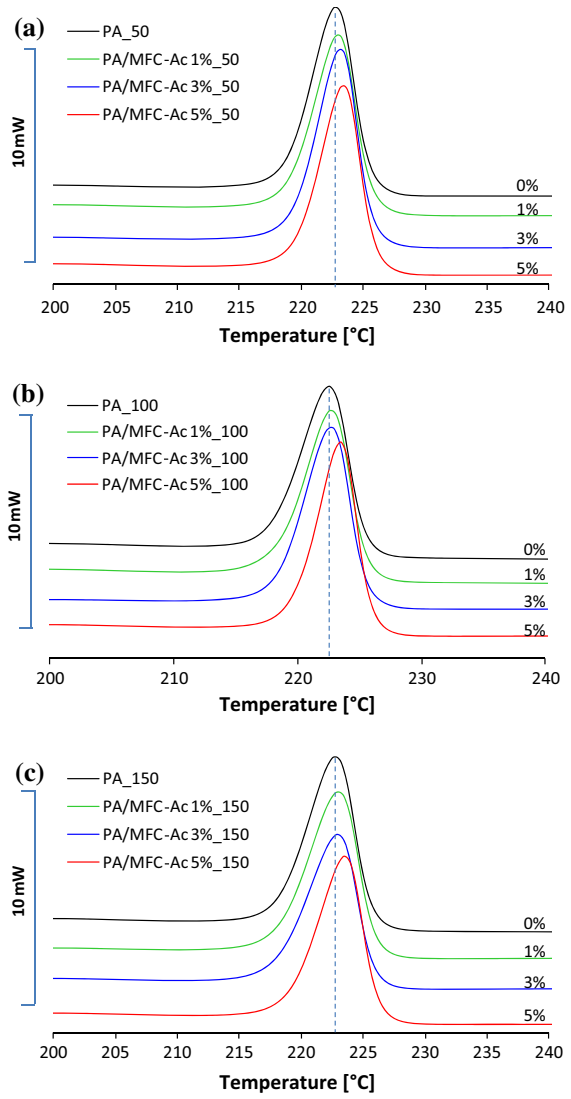

Fig. 14 DSC curves during cooling of biopolyamide composites with varying MFC-Ac content and manufactured at different screws speeds: **a** 50 rpm, **b** 100 rpm, **c** 150 rpm

where X_{cDSC}—crystallinity degree of polyamide calculated from the DSC measurements, ΔH_m—measured enthalpy of melting, ϕ—mass content of filler (Torbati et al. 2014; Virtanen et al. 2014).

Since the enthalpy of fusion of 100 % crystalline PA4.10 is not reported in literature the enthalpy of fusion of 100 % crystalline PA6.10 ($\Delta H_m^0 = 197$ J/g) was taken (Elzein et al. 2002). It is noteworthy that the heat of fusion for the totally crystalline PA6.6 was reported as $\Delta H_m^0 = 191.0$ J/g (Haberkorn et al. 1979). We assume thus that ΔH_m^0 of PA4.10 is close to the values determined for its homologous aliphatic polyamides. Crystallinity degree of PA4.10 in composite was comparable to that determined for neat sample. Subtle variations were observed that are not expected to influence the final properties of composites.

Dynamic mechanical analysis of PA4.10/MFC-Ac composites

Dynamic mechanical analysis was used to evaluate viscoelastic properties of polyamide 4.10/MFC-Ac

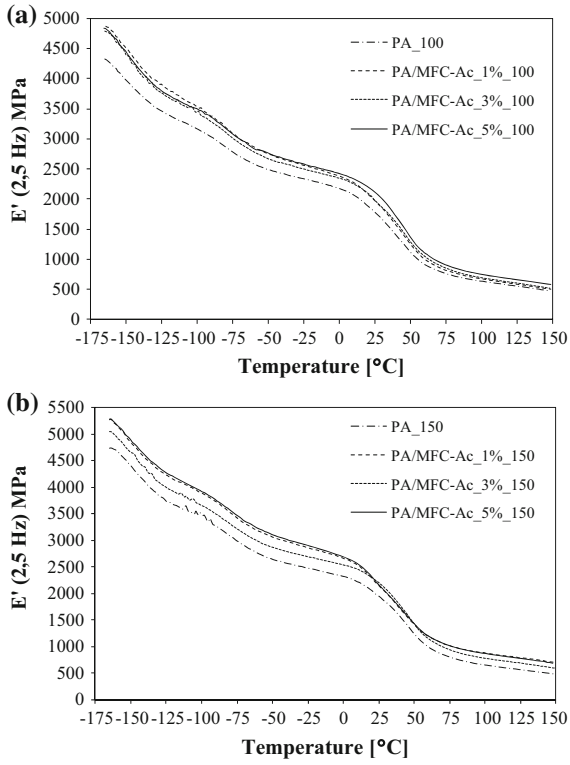

Fig. 15 Storage modulus for PA4.10/MFC-Ac composites prepared at screw speed of **a** 100 and **b** 150 rpm

composites as a function of temperature. The mechanical properties of composites showed dependence on the processing conditions that influenced structure and morphology of composites. Storage modulus E′ of all composite materials was higher than that of pure polymer in the whole temperature range (Fig. 15). For a series obtained at 100 rpm, the E′ modulus gradually increased with larger filler content. The highest increase of the storage modulus was observed for composites prepared at the highest applied rotational screw speed, *i.e.* 150 rpm (Fig. 16). The measured storage modulus of composites reflected the dispersion state of MFC and the presence of structural defects. Blending MFC at only 50 rpm did not provide good composite structure and developed numerous cavities. These structural defects led to deterioration of mechanical properties as compared to reference biopolyamide. Importantly, a higher increase of E′ was observed below glass transition temperature, *i.e.* in the temperature range of most polyamide applications. For example, the storage modulus at 25 °C increased from 1934 GPa for PA4_150 to 2199 GPa

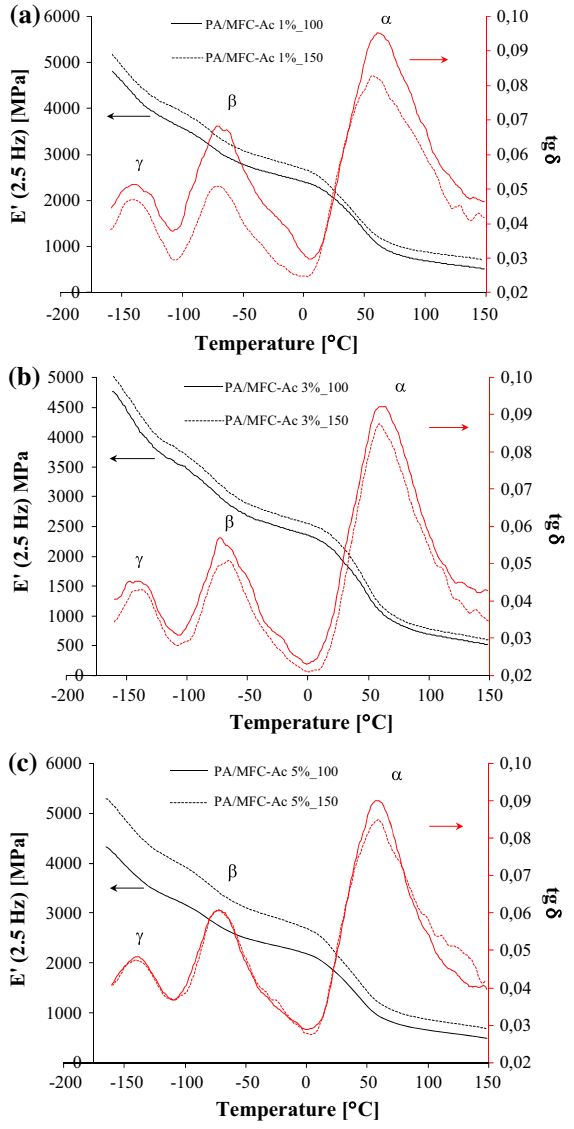

Fig. 16 Influence of processing conditions on storage modulus (E′) and tg of loss angle (tgδ) of (PA4.10/MFC-Ac composites with different MFC-Ac content of **a** 1, **b** 3 and **c** 5 wt%

for PA/MFC-Ac 3 %_150 and 2130 GPa for PA/MFC-Ac 5 %_150 sample. On the contrary to glassy state of material, the rubbery plateau of composites showed moderate improvement of storage modulus. The mechanical performance of polymer/MFC nanocomposites can be influenced by the crystalline phase of polymer matrix. For example, Suryanegara et al. obtained clearly higher values of tensile modulus and tensile strength of crystalline PLA/microfibrillated cellulose composites as compared to that of

amorphous PLA/MFC system (Suryanegara et al. 2009). Moreover, composites based on crystalline polymer matrix exhibited higher storage modulus in the DMA tests at elevated temperatures over the glass transition of PLA. Elsewhere Braun et al. demonstrated the ability of acetylated cellulose nanowhiskers to act as nucleants for PLA crystallization. The reduction of the crystallization half-time as well as increase of the crystallinity degree of PLA was reported (Braun et al. 2012). In the work by Siqueira et al. the crystallinity of PCL was increased by addition of sisal whiskers modified with n-octadecyl isocyanate while it was almost not influenced by the presence of microfibrillated cellulose bearing the same functional groups (Siqueira et al. 2009). Interestingly, although the crystallinity of MFC-based nanocomposite films was lower as compared to whiskers-based composites, the stiffness of the former was higher. This comparative study indicated the prevalent role of the entanglement in strengthening of semicrystalline polymers by cellulosic nanoparticles. In our work little variations were observed in the crystallinity degree of PA4.10 in all nanocomposites as compared to unmodified polymer (Table 4). Thus, the improvement of mechanical performance of nanocomposites can be ascribed to the reinforcement of PA4.10 by crystalline cellulose nanofibrils with negligible contribution of self-reinforcement by crystalline phase of polyamide.

The dependence of loss tangent versus temperature (Fig. 16) demonstrates the existence of three secondary relaxations, α, β and γ. Glass transition temperature (T_g) of polyamide can be determined by α relaxation, since it is usually related to the segment movements in the amorphous region (Wang and Zhang 2009). The β relaxation is ascribed to the mobility of the carbonyl group in the amorphous region and the γ relaxation is believed to reflect co-movement of amide and methane groups.

The α transition temperature was slightly affected by the addition of MFC-Ac and by the processing conditions (Fig. 16). The T_g determined for pure PA4.10_100 and PA4.10_150 did not change much and it was 58.5 and 57.7 °C, respectively. For the composites with up to 3 wt% content of MFC-Ac processed at 100 rpm the T_g value was not influenced as compared to the extruded PA4.10 and oscillated around 58 °C. However, for the composites that were processed at higher screw speed (150 rpm), the α transition temperature was slightly shifted towards lower temperatures as compared to unmodified PA4.10. For the composites containing 5 wt% of MFC-Ac the α transition temperatures were lowered by *ca.* 3 °C regardless of the applied rotational screw speed. In these materials larger interfacial surface might be produced due to higher content of the filler. Complex physical processes with opposite effects could contribute to the final performance of relaxation phenomena in the polymer composites. Firstly, the observed changes could result from the plasticizing effect of acetyl moieties which were located on the surface of modified MFC. For example, the literature reported plasticizing of PLA by surfactant adsorbed on cellulose nanocrystals (Fortunati et al. 2012a), cellulose nanowhiskers grafted by n-octadecyl-isocyanate (Espino-Pérez et al. 2013) and lactide oligomers attached to cellulose nanowhiskers (Goffin et al. 2011). The effect of increased storage modulus and decreased glass transition temperature was found, for example, for PLA/nanocrystalline cellulose nanocomposites by Fortunati et al. (2012b). On the other hand, the polymer-filler interactions are known to have opposite effect of rendering the α relaxation of polymer matrix and shifting it towards higher temperatures (Ahn et al. 2009; Papon et al. 2012; Raftopoulos and Pielichowski 2015). Slight increase of T_g was reported for instance for acetylated cellulose nanoparticles blended with PLA (Abdulkhania et al. 2014; Lin et al. 2011). Effects related to the interfacial area depend on the filler content and degree of dispersion. More distinct changes in T_g, which were observed for 5 wt% content of MFC-Ac and nanocomposites processed at higher screw speed, probably reflect higher surface area of polymer-nanofiller interface. Lowering of T_g might also indicate more pronounced changes in the molecular weight of polymer matrix exposed to high shearing forces as compared to that processed under moderate conditions. The increase of the melt viscosity of composites in relation to pristine polymers is a typical phenomenon that makes the polymeric components more prone to thermomechanical degradation. Therefore stronger changes in molecular weight of PA4.10 might be observed for composites with 5 wt% of MFC-Ac. However, the decrease of T_g with lowering polymer molecular weight, expressed by Fox–Flory equation (Gauthier 1995), is not large in the range of high molecular weight of polymer, which is the case for the commercial engineering polymers. However, a strong decrease of T_g versus mechanical

energy that was delivered to the unit mass of extruded material, as well as lowering of the average molecular weight, were reported for the amylose and amylopectin in corn flour. The distinct effect rose from extrusion-induced mechanical degradation of biopolymers (Kaletunc and Breslauer 1993). Prolonged heating applied during extrusion of PA4.10/MFC-Ac nanocomposite with melt recycle is another factor considered as a possible reason of matrix degradation. Significant reduction of molecular weight upon prolonged heating was reported for *e.g.* PLA copolymers (Garlotta 2001). Moreover, low molecular weight products formed during the thermo-mechanical degradation of polyamide and/or cellulose might dilute in the polymer matrix, leading eventually to the plasticization of polyamide matrix. The values of polyamide's T_g is also sensitive to water content which in polyamides is known to act as a plasticizer—water shifts the T_g towards lower temperatures (Murthy 2006). On the other hand, molecular orientation during bio-PA processing can also influence the glass transition temperature and, as a result, the oriented segments of polyamide relax at a higher temperature.

tgδ diagrams of all materials under investigation display a small shoulder at *ca.* −15 °C. Similar small transition peak was observed between α and β peaks of PA11.11 and was defined as β_c relaxation related to the absorbed water (Liu and Zhao 2014).

Conclusions

This work demonstrated that thermal stability enhancements of modified crystalline cellulose can be achieved by proper modification and this modified bioadditive can be considered as a useful filler for biopolyamide engineering polymers with processing temperature over 200 °C. Physical treatment combined with chemical surface modification of MFC resulted in removal of less thermally stable non-cellulose components from MFC and introduction of acetyl groups that showed a stabilizing effect on the MFC filler. The prepared MFC-Ac nano/microfiller was composed of stiff fibrous particles with exposed nanocrystals. The morphology of MFC-Ac could result from the simultaneous action of chemical process of acidic hydrolysis, especially in amorphous region of cellulose, and physical disintegration, particularly of larger particles, during repeated sonification. Cellulose micro and nanofibers displayed low degree of entanglement and less intensive hydrophilic character. Changes of MFC surface properties and morphological features produced in modification procedure were favourable in terms of dispersibility of additive in bio-PA matrix. The processing parameters during melt blending of (nano)-composites of bio-polyamide and modified MFC were critical for achieving good dispersion and structure of micro/nanocomposites providing enhancement of dynamic mechanical properties. In the tested range of screw speeds it was found that at screw speed of 50 rpm the shearing forces were insufficient for dispersing MFC agglomerates and low pressure did not force evacuation of gases introduced to plasticizing system of extruder with MFC-Ac aerogel.

The highest improvement of storage modulus was observed for micro/nanocomposites containing 5 wt% of MFC-Ac and processed at screw speed of 150 rpm. SEM microphotographs of nanocomposites suggested disintegration of fibrous aggregates of cellulose nanocrystals to individual nanoparticles that proceeded under shearing forces at screw speed at least 100 rpm. The DSC measurements demonstrated changes in parameters of fusion indicating formation of hydrogen bonds between components. The interfacial interactions favour stress transfer between the polymer matrix and reinforcing filler and are crucial for the mechanical performance of these new 'green' composites.

Acknowledgments Authors are grateful to the Polish National Science Center for financial support under Contract No. DEC-2011/01/M/ST8/06834. The company J. Rettenmaier and Söhne Gmbh+Co.Kg is kindly acknowledged for sending samples of MFC used in this work. Dr. Joanna Pagacz and M.Sc. Oskar Bartyzel are acknowledged for help during testing materials.

References

Abdulkhania A, Hosseinzadeha J, Ashorib A, Dadashic S, Takzare Z (2014) Preparation and characterization of modified cellulose nanofibers reinforced polylactic acid

nanocomposite. Polym Test 35:73–79. doi:10.1016/j.polymertesting.2014.03.002

Afshari M, Gupta A, Jung D, Kotek R, Tonelli AE, Vasanthan N (2008) Properties of films and fibers obtained from Lewis acid–base complexed nylon 6,6. Polymer 49(5):1297–1304. doi:10.1016/j.polymer.2008.01.038

Ahn SI, Ohk CW, Kim JH, Zin W-C (2009) Glass transition temperature of polymer nanocomposites: prediction from the continuous-multilayer model. J Polym Sci Part B Polym Phys 47(22):2281–2287. doi:10.1002/polb.21826

Ali M, Emsley AM, Herman H, Heywood RJ (2001) Spectroscopic studies of the ageing of cellulosic paper. Polymer 42:2893–2900. doi:10.1016/S0032-3861(00)00691-1

Braun B, Dorgan J (2009) Single-step method for the isolation and surface functionalization of cellulosic nanowhiskers. Biomacromolecules 2:334–341. doi:10.1021/bm8011117

Braun B, Dorgan JR, Hollingsworth LO (2012) Supra-molecular ecobionanocomposites based on polylactide and cellulosic nanowhiskers: synthesis and properties. Biomacromolecules 13:2013–2019. doi:10.1021/bm300149w

Builes DH, Labidi J, Eceiza A, Mondragon I, Tercjak A (2013) Unsaturated polyester nanocomposites modified with fibrillated cellulose and PEO-b-PPO-b-PEO block copolymer. Compos Sci Technol 89:120–126. doi:10.1016/j.compscitech.2013.09.015

DSM (2014) Technical data sheet of EcoPaXX Q170 MS; http://www.dsm.com/products/ecopaxx/en_US/product-info/product-data-sheets.html. Accessed 12 Nov 2014

Dufresne A (2012) Nanocellulose: from nature to high performance tailored materials. Walter de Gruyter GmbH, Berlin/Boston

Elzein T, Brogly M, Schultz J (2002) Crystallinity measurements of polyamides adsorbed as thin films. Polymer 43:4811–4822. doi:10.1016/S0032-3861(02)00239-2

Espino-Pérez E, Bras J, Ducruet V, Guinault A, Dufresne A, Domenek S (2013) Influence of chemical surface modification of cellulose nanowhiskers on thermal, mechanical, and barrier properties of poly(lactide) based bionanocomposites. Eur Polym J 49:3144–3154. doi:10.1016/j.eurpolymj.2013.07.017

Eyley S, Thielemans W (2014) Surface modification of cellulose nanocrystals. Nanoscale 6:7764–7779. doi:10.1039/C4NR01756K

Fengel D (1993) Influence of water on the OH valency range in deconvoluted FTIR spectra of cellulose. Holzforschung 47:103–108

Fortunati E, Armentano I, Zhou Q, Iannoni A, Saino E, Visai L, Berglund LA, Kenny JM (2012a) Multifunctional bionanocomposite films of poly(lactic acid), cellulose nanocrystals and silver nanoparticles. Carbohydr Polym 87(2):1596–1605. doi:10.1016/j.carbpol.2011.09.066

Fortunati E, Armentano I, Zhou Q, Puglia Terenzi A, Berglund LA, Kenny JM (2012b) Microstructure and nonisothermal cold crystallization of PLA composites based on silver nanoparticles and nanocrystalline cellulose. Polym Degrad Stab 97:2027–2036. doi:10.1016/j.polymdegradstab.2012.03.027

Fraschini C, Chauve G, Le Berre J-F, Ellis S, Méthot M, O'Connor B, Bouchard J (2014) Critical discussion of light scattering and microscopy techniques for CNC particle sizing. Nord Pulp Paper Res J 29(1):31–40

French AD, Cintrón MS (2013) Cellulose polymorphy, crystallite size, and the Segal Crystallinity Index. Cellulose 20:583–588. doi:10.1007/s10570-012-9833-y

Gamelas JAF, Pedrosa J, Lourenço AF, Mutjé P, González I, Chinga-Carrasco G, Singh G, Ferreira PJT (2015) On the morphology of cellulose nanofibrils obtained by TEMPO-mediated oxidation and mechanical treatment. Micron 72:28–33. doi:10.1016/j.micron.2015.02.003

Garlotta D (2001) A literature review of poly(lactic acid). J Polym Environ 9(2):63–84. doi:10.1023/A:1020200822435

Gauthier M (ed) (1995) Engineered materials handbook desk edition, section 5: testing and characterization of polymeric materials. Novelty, ASM International, pp 367–392

Gierlinger N, Schwanninger M, Reinecke A, Burgert I (2006) Molecular changes during tensile deformation of single wood fibers followed by Raman microscopy. Biomacromolecules 7(7):2077–2081. doi:10.1021/bm060236g

Goffin A-L, Raquez J-M, Duquesne E, Siqueira G, Habibi Y, Dufresne A, Dubois P (2011) From interfacial ring-opening polymerization to melt processing of cellulose nanowhisker-filled polylactide-based nanocomposites. Biomacromolecules 12(7):2456–2465. doi:10.1021/bm200581h

Haberkorn H, Illers KH, Simak P (1979) Molekiilordnung und Kristallinitäit in Polyhexamethylenadipamid. Colloid Polym Sci 257:820–840

He Y, Asakawa N, Li J, Inoue Y (2001a) Effects of low molecular weight compounds with hydroxyl groups on properties of poly(L-lactic acid). J Appl Polym Sci 82:640–649. doi:10.1002/app.1892

He Y, Li J, Uyama H, Kobayashi S, Inoue Y (2001b) Hydrogen-bonding interaction and miscibility between poly(ε-caprolactone) and enzymatically polymerized novel polyphenols. J Polym Sci Part B Polym Phys 39(22):2898–2905. doi:10.1002/polb.10044

He Y, Zhu B, Inoue Y (2004) Hydrogen bonds in polymer blends. Prog Polym Sci 29:1021–1051. doi:10.1016/j.progpolymsci.2004.07.002

Hinterstoisser B, Salmén L (2000) Application of dynamic 2D FTIR to cellulose. Vib Spectrosc 22:111–118. doi:10.1016/S0924-2031(99)00063-6

Kaletunc G, Breslauer KJ (1993) Glass transitions of extrudates: relationship with processing-induced fragmentation and end-product attributes. Cereal Chem 70(5):548–552

Kasaliwal GR, Göldel A, Pötschke P, Heinrich G (2011a) Influences of polymer matrix melt viscosity and molecular weight on MWCNT agglomerate dispersion. Polymer 52(4):1027–1036. doi:10.1016/j.polymer.2011.01.007

Kasaliwal GR, Villmow T, Pegel S, Potschke P (2011b) Influence of material and processing parameters on carbon nanotube dispersion in polymer melts. In: McNally T, Pötschke P (eds) Polymer-carbon nanotube composites: preparation, properties and applications. Woodhead Publishing Limited, Cambridge, p 128

Leppänen K, Andersson S, Torkkeli M, Knaapila M, Kotelnikova N, Serimaa R (2009) Structure of cellulose and microcrystalline cellulose from various wood species, cotton and flax studied by X-ray scattering. Cellulose 16(6):999–1015. doi:10.1007/s10570-009-9298-9

Leszczyńska A, Pielichowski K, Justin R, Chen B (2013) Surface modification of microfibrillated cellulose by

heterogeneous acetylation for bio-based polyamide composites. Mod Pol Mater Environ Appl 5:319–330
Li J, He Y, Ishida K, Yamane T, Inoue Y (2001) The hydrogen-bonding interactions between 4,4'-thiodiphenol and some poly(hydroxyalkanoic acid)s revealed by DSC and FT-IR spectroscopic analysis. Polym J 33:773–782. doi:10.1295/polymj.33.773
Lin N, Huang J, Chang PR, Feng J, Yu J (2011) Surface acetylation of cellulose nanocrystal and its reinforcing function in poly(lactic acid). Carbohydr Polym 83:1834–1842. doi:10.1016/j.carbpol.2010.10.047
Lindner B, Petridis L, Langan P, Smith JC (2015) Determination of cellulose crystallinity from powder diffraction diagrams. Biopolymers 103(2):67–73. doi:10.1002/bip.22555
Liu S, Zhao Q (2014) Characterizing petroleum fermentation polyamide 11,11. Soc Plast Eng Plast Res Online. doi:10.2417/spepro.005347
Luo J, Zhou T, Fu X, Liang H, Zhang A (2011) Mechanism in Brill transition of polyamide 66 studied by two-dimensional correlation infrared spectroscopy. Eur Polym J 47:230–237. doi:10.1016/j.eurpolymj.2010.11.017
Miao C, Hamad WY (2013) Cellulose reinforced polymer composites and nanocomposites: a critical review. Cellulose 20:2221–2262. doi:10.1007/s10570-013-0007-3
Missoum K, Belgacem MN, Bras J (2011) Nanofibrillated cellulose surface modification: a review. Materials 6:1745–1766. doi:10.3390/ma6051745
Morán JI, Alvarez VA, Cyras VP, Vázquez A (2008) Extraction of cellulose and preparation of nanocellulose from sisal fibers. Cellulose 15:149–159. doi:10.1007/s10570-007-9145-9
Murthy NS (2006) Hydrogen bonding, mobility, and structural transitions in aliphatic polyamides. J Polym Sci Part B Polym Phys 44:1763–1782. doi:10.1002/polb.20833
Niaounakis N (2015) Biopolymers: processing and products. Elsevier, Oxford, p 25
Nogi M, Abe K, Handa K, Nakatsubo F, Ifuku S, Yano H (2006) Property enhancement of optically transparent bionanofiber by acetylation. Appl Phys Lett 89:233123/1–233123/3. doi:10.1063/1.2403901
Ogava T, Fujiwara S (eds) (1985) Handbook of polymer analysis. Japan Society for Analytical Chemistry, Tokyo, p 321
Papon A, Montes H, Hanafi M, Lequeux F, Guy L, Saalwächter K (2012) Glass-transition temperature gradient in nanocomposites: evidence from nuclear magnetic resonance and differential scanning calorimetry. Phys Rev Lett 108:065702. doi:10.1103/PhysRevLett.108.065702
Park S, Baker JO, Himmel ME, Parilla PA, Johnson DK (2010) Cellulose crystallinity index: measurement techniques and their impact on interpreting cellulase performance. Biotechnol Biofuels 3:10. doi:10.1186/1754-6834-3-10
Qua EH, Hornsby PR, Sharma HSS, Lyons G (2011) Preparation and characterization of cellulose nanofibers. J Mater Sci 46:6029–6045. doi:10.1007/s10853-011-5565-x
Raftopoulos KN, Pielichowski K (2015) Segmental dynamics in hybrid polymer/POSS nanomaterials. Prog Polym Sci (in press); ttp://dx.doi.org/10.1016/j.progpolymsci.2015.01.003
Rettenmaier J, Söhne Gmbh+Co.Kg (2012) Technical data sheet of Arbocell. 40-10
Roberts MF, Jenekhe SA (1991) Site-specific reversible scission of hydrogen bonds in polymers: an investigation of polyamides and their Lewis acid-base complexes by infrared spectroscopy. Macromolecules 24:3142–3146. doi:10.1021/ma00011a017
Rodionova G, Lenes M, Eriksen Ø, Gregersen Ø (2011) Surface chemical modification of microfibrillated cellulose: improvement of barrier properties for packaging applications. Cellulose 18:127–134. doi:10.1007/s10570-010-9474-y
Segal L, Creely JJ, Martin AE Jr, Conrad CM (1959) An empirical method for estimating the degree of crystallinity of native cellulose using the X-ray diffractometer. Text Res J 29(10):786–794
Siqueira G, Bras J, Dufresne A (2009) Cellulose whiskers versus microfibrils: influence of the nature of the nanoparticle and its surface functionalization on the thermal and mechanical properties of nanocomposites. Biomacromolecules 10:425–432. doi:10.1021/bm801193d
Suryanegara L, Nakagaito AN, Yano H (2009) The effect of crystallization of PLA on the thermal and mechanical properties of microfibrillated cellulose-reinforced PLA composites. Compos Sci Technol 69:1187–1192. doi:10.1016/j.compscitech.2009.02.022
Terinte N, Ibbett R, Schuster KC (2011) Overview on native cellulose and microcrystalline cellulose I structure studied by X-ray diffraction (WAXD): comparison between measurement techniques. Lenzinger Berichte 89:118–131
Torbati AH, Birjandi Nejad H, Ponce M, Sutton JP, Mather PT (2014) Properties of triple shape memory composites prepared via polymerization-induced phase separation. Soft Matter 10:3112–3121. doi:10.1039/C3SM52599F
Virtanen S, Vartianen J, Setälä H, Tammelin T, Vuoti S (2014) Modified nanofibrillated cellulose–polyvinyl alcohol films with improved mechanical performance. RSC Adv 4:11343–11350. doi:10.1039/C3RA46287K
Wang W-Z, Zhang Y-H (2009) Environment-friendly synthesis of long chain semiaromatic polyamides. Express Polym Lett 3(8):470–476. doi:10.3144/expresspolymlett.2009.58
Zhu B, He Y, Yoshie N, Asakawa N, Inoue Y (2004) Partial phase segregation in strongly hydrogen-bonded and miscible blends. Macromolecules 37:3257–3266. doi:10.1021/ma035889t